# Evaluation of an Independent Linear Model for Acoustic Noise on a Conventional MRI Scanner and Implications for Acoustic Noise Reduction

Ziyue Wu,[1,2]* Yoon-Chul Kim,[1] Michael C.K. Khoo,[2] and Krishna S. Nayak[1]

**Purpose:** To evaluate an independent linear model for gradient acoustic noise on a conventional MRI scanner, and to explore implications for acoustic noise reduction in routine imaging.

**Methods:** Acoustic noise generated from each physical gradient axis was modeled as the prescribed gradient waveform passed through a linear time-invariant system. Homogeneity and superposition properties were experimentally determined. We also developed a new method to correct relative time shifts between the measured impulse responses for different physical gradient axes. Model accuracy was determined by comparing predicted and measured sound using normalized energy difference. Transfer functions were also measured in subjects with different body habitus and at multiple microphone locations.

**Results:** Both superposition and homogeneity held for each physical gradient axis with errors less than 3%. When all gradients were on simultaneous sound prediction, error was reduced from 32% to 4% after time-shift correction. Transfer functions also showed high sensitivity to body habitus and microphone location.

**Conclusion:** The independent linear model predicts MRI acoustic noise with less than 4% error. Acoustic transfer functions are highly sensitive to body habitus and position within the bore, making it challenging to produce a general approach to acoustic noise reduction based on avoiding system resonance peaks. **Magn Reson Med 71:1613–1620, 2014. © 2013 Wiley Periodicals, Inc.**

**Key words:** acoustic noise; MRI; transfer function; frequency response; noise reduction

## INTRODUCTION

Acoustic noise, caused by fluctuating gradient magnetic fields, is a significant source of patient discomfort in routine clinical MRI. This issue is more significant at higher field strength (1) and can exceed 130 dBA in extreme cases on commercial 3T scanners by our measurement. This problem becomes more severe for long scans, and situations where it is desirable for the subject to sleep without sedation during MRI scanning (2,3).

MRI acoustic noise originates from vibrations of the three pairs of physical gradient coils. Because these coils are inside a large static magnetic field ($B_0$), they will experience Lorentz forces when the currents in these coils change (slewing). MRI scans require constant switching of the gradients to generate spatial information. This leads to constant changes in Lorentz forces, which cause vibrations of the gradient coils. The noise can be heard because these vibrations occur at frequencies within audible range (20–20 kHz).

Many attempts have been made to characterize and reduce MRI acoustic noise (4–15). These include active noise cancellation during gradient design (4); inserting a vacuum layer to isolate vibration propagation (5); installing extra copper shielding to increase shielding efficacy (6); analyzing the impact of inserting a gradient coil on vibration with a finite element model (7); and exploring trade-offs between acoustic noise and field linearity during coil design (8,9). An independent linear model was first proposed by Hedeen and Edelstein (10), in which a transfer function relates the input gradient waveform and output acoustic noise on each of the three gradient axes. Several other studies followed this model (11–18). The transfer functions were measured and used to design "soft" gradients (11) and study $B_0$ fluctuation caused by gradient coil vibrations (12). Smink et al. (13) showed the ability to reduce sound pressure level (SPL) by adjusting repetition time (TR) to avoid resonance peaks of the scanner. Schmitter and Bock (14) modified slice-select gradient shape to avoid acoustic resonance frequencies (14). Li et al. (15) demonstrated prediction of the sound of echo planar imaging sequences based on the transfer functions mainly from one physical axis. Shaping and timing of the gradient pulses were both taken into consideration in Ref. (16), but the results were still limited to one axis only. Measurements from all the three gradient axes were combined and used to predict acoustic noise for different sequences in Refs. (17) and (18), but the results showed substantial difference between predicted and recorded sound. The differences were more than 20 dB at some frequencies.

In this work, we experimentally evaluate the independent linear model for gradient-induced acoustic noise, by directly testing the superposition and homogeneity properties. We also introduce a new method to synchronize the measured impulse responses for all gradient axes and demonstrate significantly improved sound prediction when multiple gradients are used simultaneously. Finally, we examine differences in the measured transfer

[1]Ming Hsieh Department of Electrical Engineering, University of Southern California, Los Angeles, California, USA.

[2]Department of Biomedical Engineering, University of Southern California, Los Angeles, California, USA.

Grant sponsor: National Institute of Health; Grant number: NIH R01-HL105210.

*Correspondence to: Ziyue Wu, 3740 McClintock Avenue, EEB 400, University of Southern California, Los Angeles, CA 90089-2564, USA. E-mail: ziyuewu@usc.edu

Received 16 February 2013; revised 10 April 2013; accepted 17 April 2013

DOI 10.1002/mrm.24798

Published online 11 June 2013 in Wiley Online Library (wileyonlinelibrary.com).

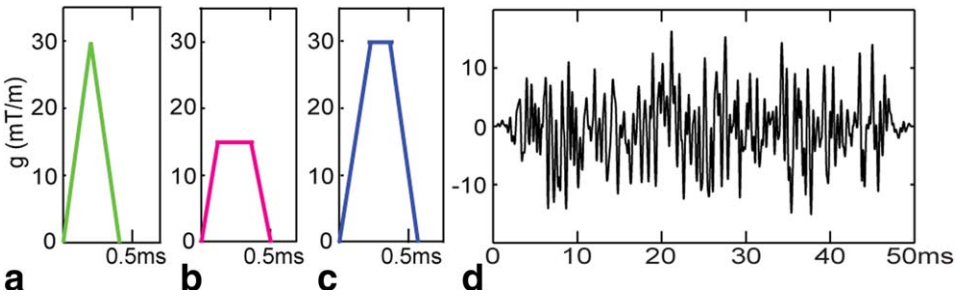


FIG. 1. Representative gradient waveforms used for linearity test and transfer function measurement. (a)–(c) are triangle and trapezoids; (d) shows one realization of random noise gradient after low-pass filtering ($f_c$ = 4 kHz) and 10 different realizations are used. For superposition test, any two of the waveforms are first scaled by 1/2 and then summed to make sure maximum slew rate is not exceeded. The units for these waveforms are all mT/m. [Color figure can be viewed in the online issue, which is available at wileyonlinelibrary.com.]

functions with different subjects and different microphone locations within the scanner bore for a single subject, and discuss implications on the ability to perform general acoustic noise reduction by avoiding system resonance peaks.

## METHODS

### Experimental Methods

Experiments were performed on a clinical 3T MR scanner (EXCITE HDxt, General Electric, Waukesha, WI). Gradient waveforms were designed in MATLAB (MathWorks Inc., Natick, MA), based on a maximum amplitude of 40 mT/m, maximum slew rate of 150 mT/m/ms, and sampling period of 4 μs. Gradient waveforms included the following: triangles, trapezoids, and low-pass filtered random noise. Acoustic noise was recorded using an MRI-compatible microphone (Model 4189, Brüel & Kjær, Nærum, Denmark). We used the highest sample rate (48 kHz) available on the device. SPL was measured using a sound level meter (Model 2250, Brüel & Kjær).

### Single-Axis Linearity Testing and Transfer Functions

Previous studies (10–18) have assumed that, for each pair of gradient coils, there is a linear system relationship between the gradient waveforms and the acoustic noise they produced. To our knowledge, this linear relationship has not yet been verified by direct experiment based on the definition of linearity. We begin by directly testing the homogeneity and superposition properties of each axis.

Let $T\{\cdot\}$ be the system function where the input $g_i(t)$ ($i$ = x, y, z) is the gradient waveform and output $y_i(t)$ ($i$ = x, y, z) is the recorded sound. Because Fourier transform (FT) is a linear operator, homogeneity and superposition properties for each axis can be expressed as:

$$\mathrm{FT}\{T\{ag_i(t)\}\} = \mathrm{FT}\{ay_i(t)\} = aY_i(f) \quad [1]$$

$$\mathrm{FT}\{T\{g_{i,1}(t) + g_{i,2}(t)\}\} = \mathrm{FT}\{y_{i,1}(t) + y_{i,2}(t)\} = Y_{i,1}(f) + Y_{i,2}(f) \quad [2]$$

where $Y_i(f)$ is the sound spectrum of $y_i(t)$ after FT. We used triangle, trapezoidal, and 10 different filtered random noise waveforms as inputs to test system linearity on each gradient axis, as shown in Figure 1. All random noise gradient waveforms were low-pass filtered to 4 kHz due to the slew rate limit of the scanner. Homogeneity errors $e_h$ and superposition errors $e_s$ were calculated by comparing the magnitude of the right and left side of Eqs. [1] and [2], respectively: $e_h = |\mathrm{FT}\{T\{ag_i\}\} - aY_i|/|aY_i|$; $e_s = |\mathrm{FT}\{T\{g_{i,1} + g_{i,2}\}\} - (Y_{i,1} + Y_{i,2})|/|Y_{i,1} + Y_{i,2}|$.

If the linearity property holds, we can determine the system transfer functions. We define $H_i(f) = \mathrm{FT}\{y_i(t)\}/\mathrm{FT}\{g_i(t)\} = Y_i(f)/G_i(f)$ ($i$ = x, y, z) as the transfer functions, where $f$ is the temporal frequency variable. We again used the gradients shown in Figure 1 as inputs to calculate $H_i(f)$ for each axis, respectively.

### Acoustic Noise Prediction

The measured transfer functions can then be combined to predict acoustic noise $\hat{Y}(f)$ of arbitrary gradient sequence:

$$\hat{Y}(f) = G_x(f)H_x(f) + G_y(f)H_y(f) + G_z(f)H_z(f) \quad [3]$$

where $G_i(f)$ are the frequency spectra of input gradient waveforms.

One problem with the prediction arises from errors in the calculation of $H_i(f)$. It is very difficult to accurately identify the exact beginning of $y_i(t)$ that corresponds to a particular $g_i(t)$ due to background noise. Because each $H_i(f)$ is calculated individually, the relative time delays between the beginning of input $g_i(t)$ and output $y_i(t)$ for each axis are different. This leads to different time shifts of the impulse responses for different axes, which is equivalent to applying different linear phases to different $H_i(f)$. These different time shifts, if not corrected, will cause substantial complex sum errors when using Eq. [3]. We propose the following method to resolve this issue.

The beginning of the recorded sound waveform for each axis $y_i(0)$ is first selected by visual inspection or simple amplitude thresholding. Assume the difference between $y_i(0)$ and the actual time the first sound wavefront caused by gradients arriving the microphone is $\Delta t_x$, $\Delta t_y$, and $\Delta t_z$, respectively, for all three axes, Eq. [3] becomes:

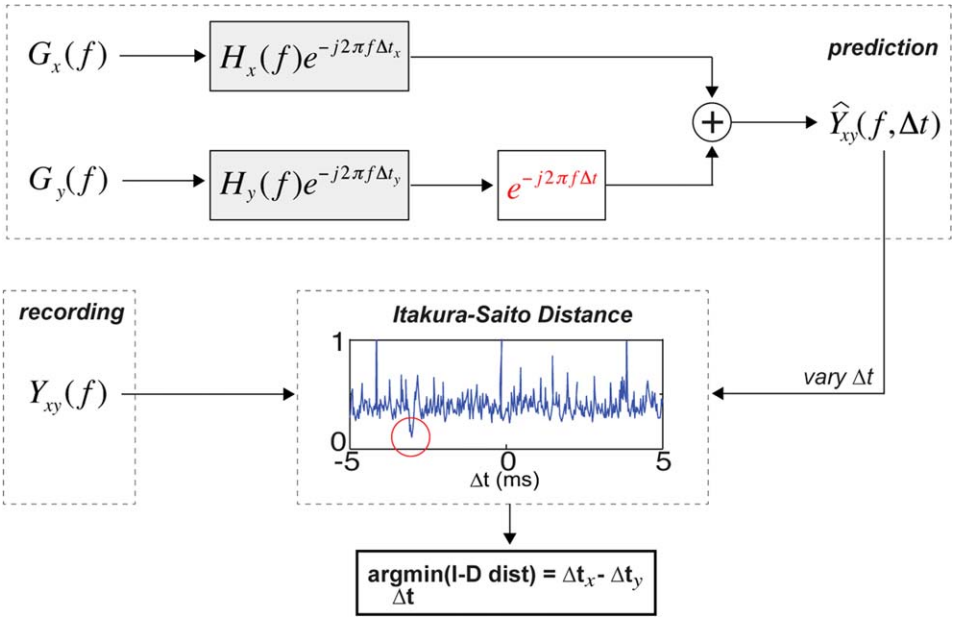


FIG. 2. Correction of time shifts for *x*- and *y*-axis impulse responses. An extra term exp $(-j2\pi\Delta t)$ is applied to $H_y(f)$ to compensate for $\Delta t_x - \Delta t_y$. Input spectra $G_x(f)$ and $G_y(f)$ are then multiplied with corresponding transfer functions and summed to produce predicted sound $\hat{Y}(f,\Delta t)$. $\hat{Y}(f,\Delta t)$ is compared with the recorded sound spectrum $Y(f)$ using Itakura-Saito distance while varying$\Delta t$. $\Delta t$ corresponding to the minimum Itakura-Saito distance is chosen as the estimate of $\Delta t_x - \Delta t_y$ and applied to future sound predictions. [Color figure can be viewed in the online issue, which is available at wileyonlinelibrary.com.]

$$\hat{Y}(f) = G_x(f)H_x(f)e^{-j2\pi f\Delta t_x} + G_y(f)H_y(f)e^{-j2\pi f\Delta t_y} + G_z(f)H_z(f)e^{-j2\pi f\Delta t_z} = e^{-j2\pi f\Delta t_x}[G_x(f)H_x(f) + G_y(f)H_y(f)e^{-j2\pi f(\Delta t_y-\Delta t_x)} + G_z(f)H_z(f)e^{-j2\pi f(\Delta t_z-\Delta t_x)}] \quad [4]$$

The exact values of $\Delta t_x$, $\Delta t_y$, and $\Delta t_z$ are difficult to determine, but if all $y_i(t)$ used to calculate $H_i(f)$ are aligned so that $\Delta t_x = \Delta t_y = \Delta t_z$, Eq. [4] is reduced to:

$$\hat{Y}(f) = e^{-j2\pi f\Delta t_x}[G_x(f)H_x(f) + G_y(f)H_y(f) + G_z(f)H_z(f)] \quad [5]$$

The linear phase term at the beginning of the right hand side of Eq. [5] would have no effect on the magnitude spectrum of $\hat{Y}(f)$ and would only cause a time shift of its corresponding time domain signal $\hat{y}(t)$. We use the following method to align $\Delta t_x$, $\Delta t_y$, and $\Delta t_z$, as described in Figure 2 as well. Arbitrary gradient inputs are played simultaneously on both *x*- and *y*-axes. An extra term exp $(-j2\pi\Delta t)$ is applied to $H_y(f)$ to compensate for the difference between $\Delta t_x$ and $\Delta t_y$. The goal is to find out $\Delta t$. Input spectra $G_x(f)$ and $G_y(f)$ are multiplied by corresponding transfer functions and summed to produce predicted sound $\hat{Y}(f,\Delta t)$. This is then compared with the recorded sound spectrum $Y(f)$ using Itakura-Saito Distance: $D_{IS}(\hat{Y},Y) = ||Y/\hat{Y} - \log(Y/\hat{Y}) - 1||_1$ (19). The smaller the distance of the two spectra, the more similar they are. If Eq. [5] holds, there should be one single minimum of $D_{IS}$ among different $\Delta t$. Thus, the $\Delta t$ corresponding to the minimum of Itakura-Saito Distance should be the difference between $\Delta t_x$ and $\Delta t_y$. The same procedure is used to align $\Delta t_x$ and $\Delta t_z$. After the different time shifts of transfer functions are aligned, we then use Eq. [5] to predict the sound.

We did experiments in two situations: (1) only one of the three gradient axes was on and (2) all the three gradients were on. The predictions were then compared with the measured acoustic noise. For comparison, we also calculated the predicted spectra with no time-shift correction being applied. All experiments above were conducted at a fixed location near isocenter when the scanner was empty.

### Dependence on Body Habitus and Microphone Location

We also investigated the impact of body habitus and microphone location on the transfer functions, as this would be critical for implementing a general method of reducing acoustic noise, e.g., one that is based on avoiding resonance peaks of the system (13,14). We measured the transfer functions when two different subjects were inside the scanner. The microphone was placed at the same location, close to the subject's left ear. Then, we moved the microphone along the axis of the bore (*z*-axis) with a distance increment of 5 cm and measured transfer functions for each gradient axis.

## RESULTS

### Single-Axis Linearity Tests and Transfer Functions

Figure 3 shows a representative example of the system homogeneity and superposition test, in which two different random noise gradients were used as inputs on the *x*-axis. The sound pressure waveforms were measured in Pascal. After applying FTs, which are integrals over time, the units become Pascal seconds. Table 1 summarizes the results for all the three axes. Homogeneity and superposition errors were within 3% for all axes, although errors for the *z*-axis were slightly higher.

Different input gradients shown in Figure 1 were used to generate transfer functions. Figure 4a–c shows calculated transfer functions for each axis, respectively. Note that the measured transfer functions did not vary with the choice of input gradient. We show the results up to 2200 Hz for the trapezoid inputs because the trapezoids we used have a full-width half-maximum of 0.4 ms,

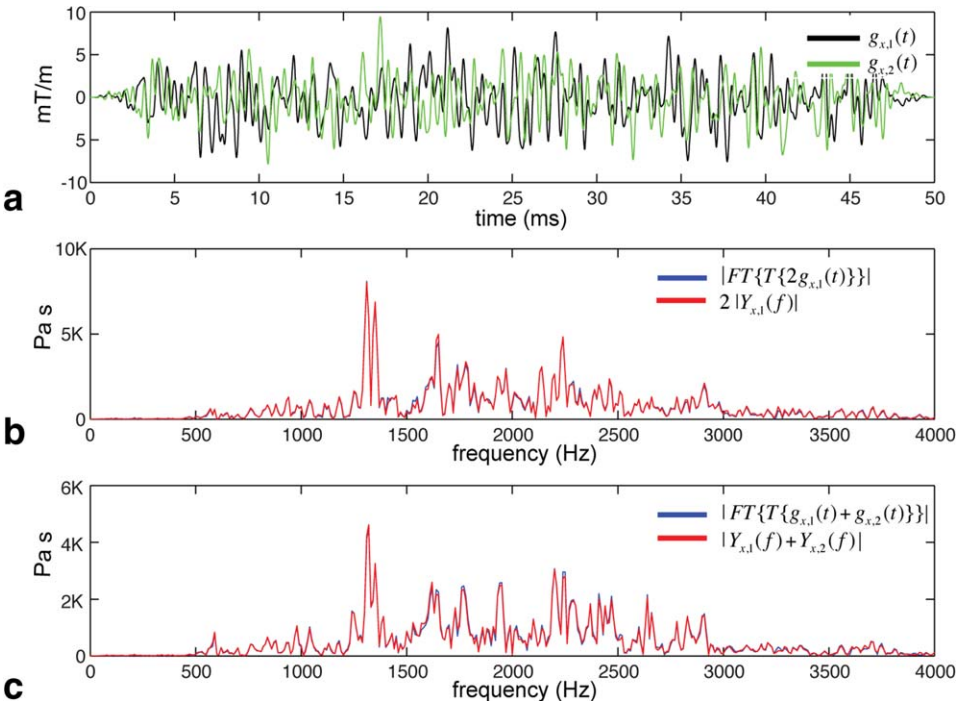


FIG. 3. One example of system homogeneity and superposition property test.(a) shows the actual random noise input gradient waveforms played after low-pass filtering. $Y_{x,1}(f)$ and $Y_{x,2}(f)$ are the recorded sound spectra for inputs $g_{x,1}(t)$ and $g_{x,2}(t)$, respectively.(b) shows homogeneity property test result based on Eq. [1] ($a = 1/2$). (c) shows superposition property test result based on Eq. [2]. The units for recorded sound pressure waveforms are Pascals (Pa), and the units for their spectra, as shown, are Pa seconds. [Color figure can be viewed in the online issue, which is available at wileyonlinelibrary.com.]

which corresponds to their first zero crossing at 2500 Hz in frequency domain. Since $H_i(f) = Y_i(f)/G_i(f)$, for any frequencies close to the zero crossings of $G_i(f)$, the value of $H_i(f)$ would not be accurate. For the same reason, we show the spectra up to 4000 Hz for the triangle input, which has its first zero crossing at 5000 Hz.

### Acoustic Noise Prediction

Table 2 summarizes our acoustic noise prediction results for each of the single axis as well as the situation where gradients were played simultaneously on all axes. Fifteen different inputs were used for each case. The predicted spectra were compared with the actual recorded sound and prediction error was calculated using power spectrum difference: $(|\hat{Y}|^2\text{-}|Y|^2)/|Y|^2\times100\%$. Two examples of prediction results are plotted in Figure 5. Figure 5a shows the case when a random noise waveform was played on *y*-axis only. Figure 5b compares the recorded and predicted sound spectra when different random noise gradients were played on all the three axes. All random noise waveforms lasted 50 ms and TR was set to 100 ms. All results were averaged over 10 TRs.

### Dependence on Body Habitus and Microphone Location

The transfer functions were also measured at a fixed location close to isocenter when two different subjects were present inside the scanner, as plotted in Figure 6. Transfer functions for four different locations next to the same subject's left ear were shown in Figure 7. The variations show random patterns that are difficult to model. To quantitatively see the impact, transfer functions measured for subject 1 were used to simulate acoustic noise when subject 2 was present; transfer function measured at one location was used to simulate sound at another location 5 cm away. The results are summarized in Table 2.

## DISCUSSION

We have tested the independent linear model for acoustic noise on a conventional MRI scanner, based on the definition of homogeneity and superposition. Our results show that this is a reasonable assumption (error $< 3\%$), especially for $g_x$ and $g_y$, where the errors are less than 1%. This is in accordance with our single axis sound prediction results. As can be seen in Table 2, the power spectrum error for the $g_z$-only case is slightly larger than for the other two axes. This may be related to the geometric assembly of the gradient coils within the scanner, which is beyond the scope of this work. But even so, the linear model is still reliable in general for each gradient axis. From Figure 4, it can be seen that for each axis, the transfer functions were input independent, which again supports the linearity of the system.

Equation 3 considers the acoustic noise produced by each pair of gradient coils to be independent. In other words, it

Table 1
Homogeneity and Superposition Property Test for Each Physical Gradient Axis

| | Homogeneity error, $e_h$ (%) | Superposition error, $e_s$ (%) |
|---|---|---|
| $g_x$ | 0.52 ± 0.13 | 0.62 ± 0.16 |
| $g_y$ | 0.48 ± 0.11 | 0.64 ± 0.15 |
| $g_z$ | 0.77 ± 0.25 | 2.77 ± 0.55 |

$$e_h = |FT\{T\{ag_i\}\} - aY_i|/|aY_i|;$$
$$e_s = |FT\{T\{g_{i,1} + g_{i,2}\}\} - (Y_{i,1} + Y_{i,2})|/|Y_{i,1} + Y_{i,2}|.$$

The input gradient waveforms used are shown in Figure 1. a was arbitrarily chosen as long as within system slew rate limit.

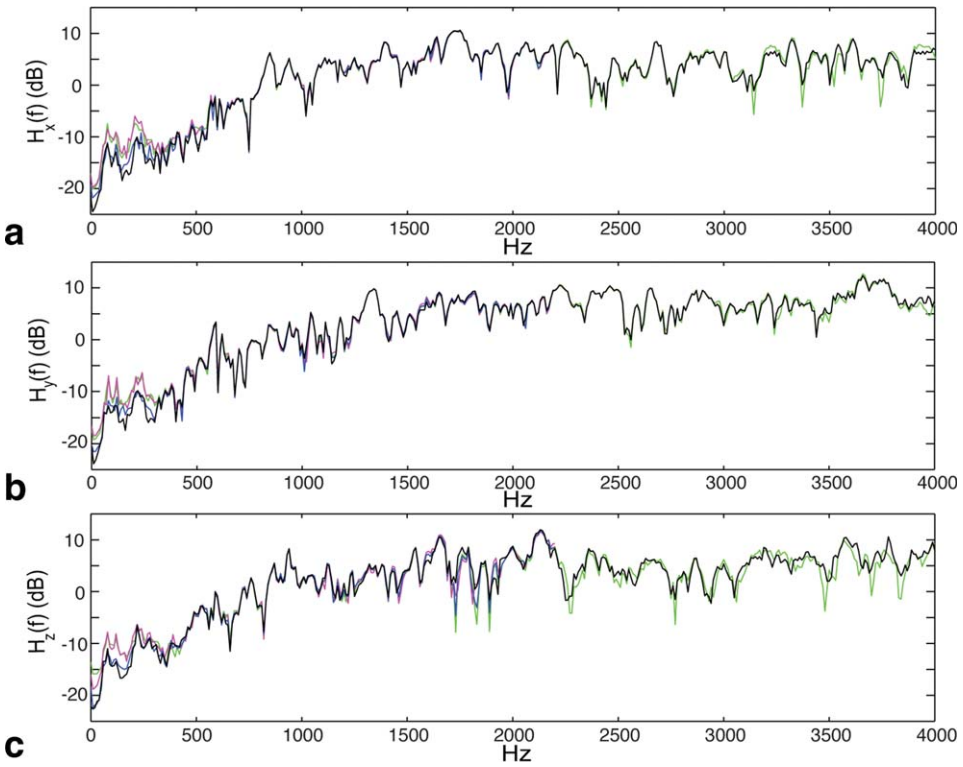


FIG. 4. Transfer functions of all the three axes. **(**a–c) shows transfer functions for *x*-, *y*-, and *z*-axis, respectively, using different gradient inputs. The colors correspond to input gradients in Figure 1. Transfer functions generated by random noise inputs were averaged over 10 different realizations. The magnitudes were referred to 0.1 Pa/(mT $m^{-1}$) as 0 dB. Note that transfer functions generated by two trapezoids were shown up to 2200 Hz due to their full-width half-maximum limits.

assumes that there is no mechanical coupling between the coils. The accuracy of this linear model depends on how the scanner is manufactured and the impact of mechanical coupling could vary among different scanner models.

Previous works (11,17,18) reported poor accuracy of the prediction methods when sound from all the three gradient axes is combined. We suspect that this is in large part due to the different time shifts of the transfer

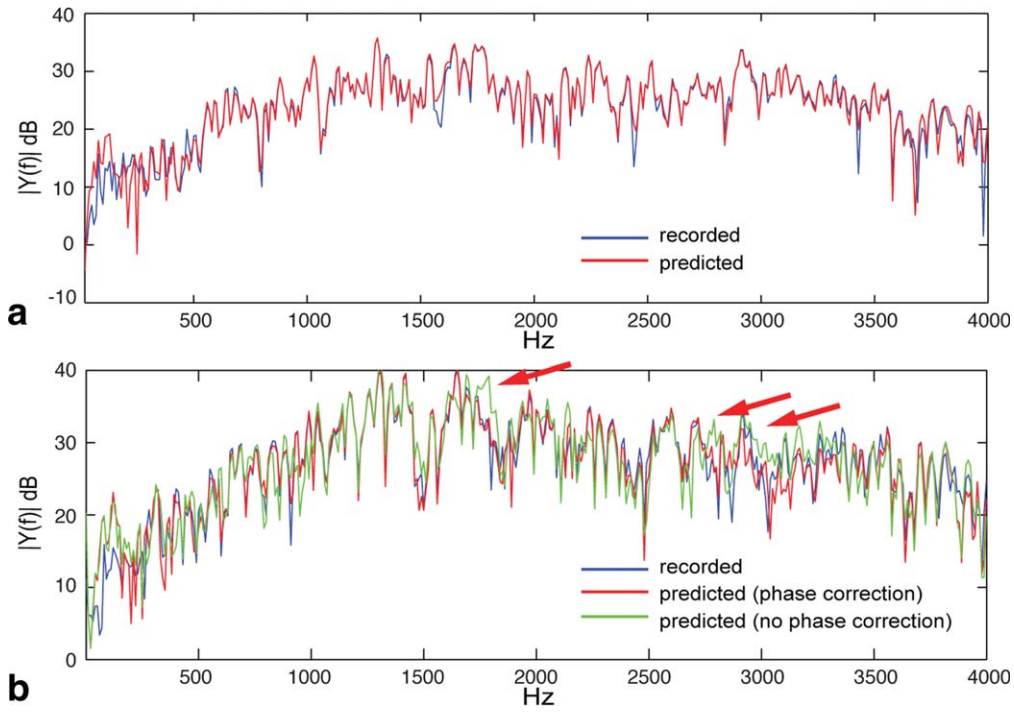


FIG. 5. Examples of predicted acoustic noise spectrum compared with recorded sound spectrum. In (a), a low-pass-filtered random noise ($f_c$ = 4 kHz) was played on *y*-axis only. In (b), different random noise gradients were played on all the three axes. All random noises waveform lasted 50 ms and TR was set to 100 ms. All results were averaged for 10 TRs. Spectrum 0 dB reference was set to 1 Pa s. The arrow points at the high-energy frequency range where the prediction without phase correction has substantial error.

Table 2
Acoustic Noise Prediction Using the Independent Linear Model

| | Prediction error (%) | Prediction error (%) (subject mismatch) | Prediction error (%) (location mismatch) |
|---|---|---|---|
| $g_x$ | 0.41 ± 0.14 | 14.97 ± 5.95 | 45.22 ± 15.32 |
| $g_y$ | 0.61 ± 0.22 | 15.23 ± 4.68 | 35.25 ± 18.38 |
| $g_z$ | 2.76 ± 1.37 | 29.36 ± 8.63 | 32.72 ± 8.32 |
| $g_x + g_y + g_z$ | 31.90 ± 6.15 | 34.52 ± 10.73 | 48.36 ± 19.57 |
| $g_x + g_y + g_z$ (with time shift correction) | 3.86 ± 2.49 | 30.11 ± 9.29 | 45.36 ± 13.77 |

Prediction error was calculated using power spectrum difference: $(|\hat{Y}|^2-|Y|^2)/|Y|^2\times100\%$.
*Subject mismatch prediction*: transfer functions measured when subject 2 was present was used for subject 1.
*Location mismatch prediction*: transfer functions measured at one location was used to predict sound at a different location 5 cm away along *z*-axis.

functions. We thus proposed a new method to align these time shifts, as mentioned in the Methods section. The prediction accuracy is substantially improved to better than 96% (Table 2). This also suggests that the impact of mechanical coupling of all gradient coils is minimal in our case and the sound generated from each gradient axis can be simply added without considering the interference between its sources.

One could argue that if a triggering device is used, the gradient pulses and sound recording can be started simultaneously. We found that the final prediction is extremely sensitive to even the smallest timing error. If any of the $y_i(t)$ used to generate transfer functions was mismatched by even two audio samples (0.04 ms), the final prediction error increased from <3% to >10%. The triggering input on our research-grade sound level meter had timing accuracy of 500 ms. A triggering device would only work if its accuracy could achieve the level of 0.01 ms or less.

It is worth noting that in Figure 5, after time shift correction, there are more errors in the lower (<300 Hz) and higher frequencies (>2800 Hz) than the frequency range between them. The lower frequency range corresponds to the wavelengths longer than 1 m, which is roughly the length of the bore. So the errors may be due to the nonlinear interference such as diffraction. Errors in higher frequency range may be due to increased sensitivity to phase. Most of the acoustic noise energy lies between 500 and 3000 Hz, which is the frequency range where the model predictions are very accurate.

Another interesting finding is that the prediction error is higher (~7%), when maximum slew rate was used on

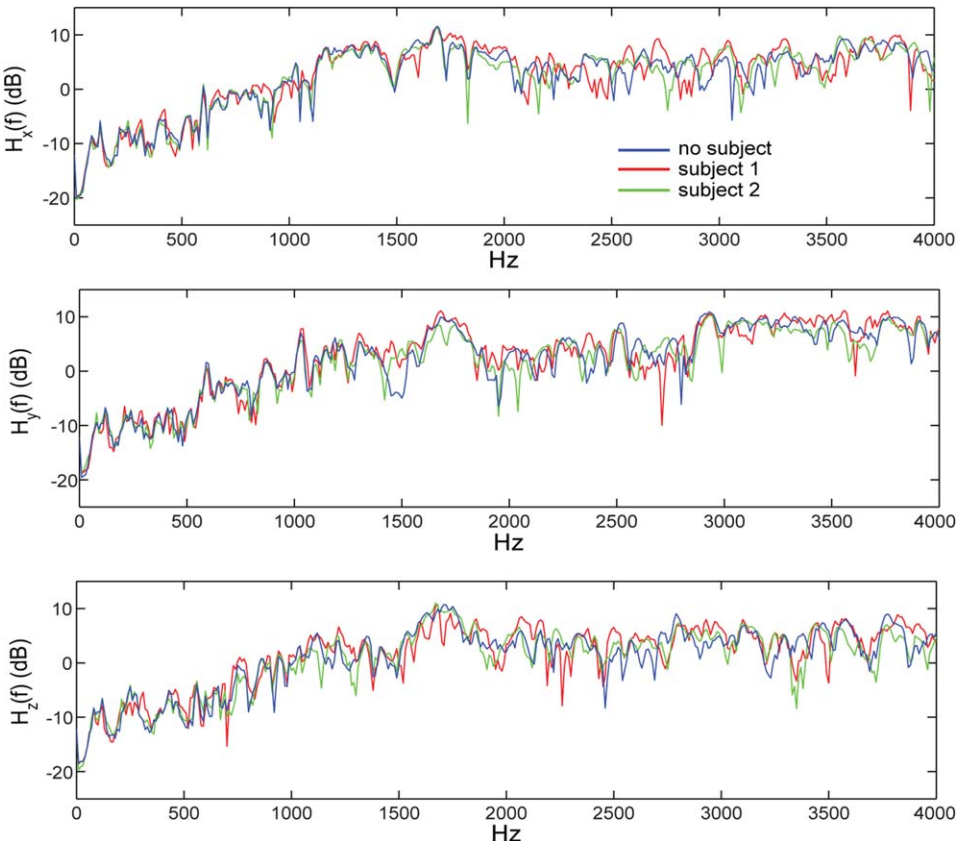


FIG. 6. Transfer functions for an empty bore and two different subjects. The microphone was placed at a fixed location close to scanner isocenter for all the three cases. 0 dB = 0.1 Pa/(mT $m^{-1}$). [Color figure can be viewed in the online issue, which is available at wileyonlinelibrary.com.]

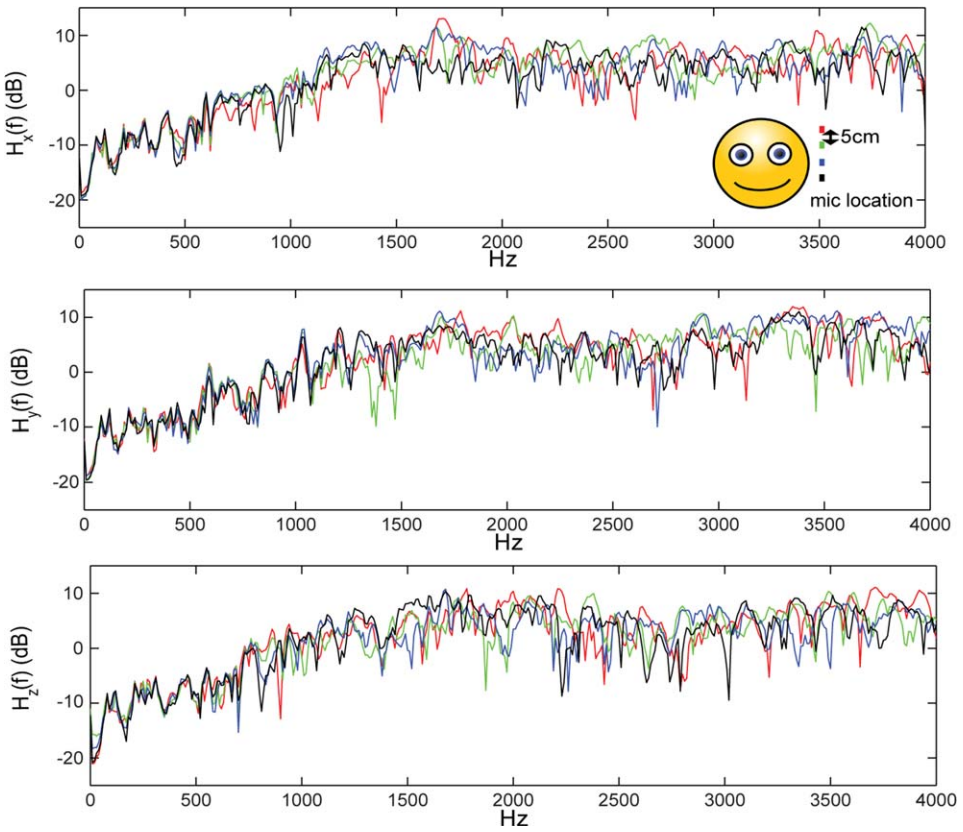


FIG. 7. Transfer functions of different microphone locations. The microphone was placed close to the subject's left ear and then moved along *z*-axis with an increment of 5 cm. 0 dB = 0.1 Pa/(mT $m^{-1}$). [Color figure can be viewed in the online issue, which is available at wileyonlinelibrary.com.]

all the three axes simultaneously. If maximum slewing does not occur at the same time or is not used, the error is roughly 3%.

With the knowledge of the transfer functions, a natural extension would be to optimize the sequence gradients to avoid the system resonance peaks so that the acoustic noise can be reduced. However, this may be difficult to implement. As we can see from Figures 6 and 7, the transfer functions vary greatly among different subjects and microphone locations, especially for frequencies higher than 1000 Hz. Table 2 also shows substantial prediction errors if the *exact* transfer functions are not used. Due to the nature of sound wave propagation and the irregular shape of scanners, the variation is difficult to model. Even if the acoustic noise at a particular location can be reduced, unless both the table and the subject are still throughout the examination, or the gradient sequence is designed such that most of the energy is located at frequencies below 1 kHz, it would be difficult for the subject to benefit.

## CONCLUSIONS

We have evaluated an independent linear model for gradient-induced MRI acoustic noise on a commercial 3T scanner by experimentally testing the superposition and homogeneity properties. The results show that the errors are less than 3% for all physical gradient axes, and less than 4% when all physical gradient axes are on simultaneously. We introduced a new method to synchronize measured acoustic impulse response for the three axes that improved prediction error from 32% to 4% when all gradients are on simultaneously. Finally, we demonstrated that the gradient-sound transfer functions are highly dependent on body habitus and microphone location within the scanner bore, suggesting that any general approaches for acoustic noise reduction based on avoiding system resonance peaks will likely require subject-specific and location-specific calibration scans.

## ACKNOWLEDGEMENTS

The authors thank Vikram Ramanarayanan and Daoming Jiang for their help with acoustic data collection.

## REFERENCES

1. Price DL, De Wilde JP, Papadaki AM, Curran JS, Kitney RI. Investigation of acoustic noise on 15 MRI scanners from 0.2 T to 3 T. J Magn Reson Imag 2001;13:288–293.
2. Ikeda K, Ogura M, Oshima T, et al. Quantitative assessment of the pharyngeal airway by dynamic magnetic resonance imaging in obstructive sleep apnea syndrome. Ann Oto Rhinol Laryn 2001;110:183–189.
3. Shin LK, Holbrook AB, Capasso R, Kushida CA, Powell NB, Fischbein NJ, Pauly KB. Improved sleep MRI at 3 Tesla in patients with obstructive sleep apnea. J Magn Reson Imag 2013. doi 10.1002/jmri.24029.
4. Mansfield P, Haywood B, Coxon R. Active acoustic control in gradient coils for MRI. Magn Reson Med. 2001;46:807–818.
5. Edelstein WA, Hedeen RA, Mallozzi RP, El-Hamamsy S-A, Ackermann RA, Havens TJ. Making MRI quieter. Magn Reson Imag 2002;20:155–163.
6. Edelstein WA, Kidane TK, Taracila V, et al. Active-passive gradient shielding for MRI acoustic noise reduction. Magn Reson Med 2005;53:1013–1017.
7. Yao GZ, Mechefske CK, Rutt BK. Vibration analysis and measurement of a gradient coil insert in a 4T MRI. J Sound Vib 2005;285:743–758.

8. Forbes LK, Brideson MA, Crozier S, While PT. An analytical approach to the design of quiet cylindrical asymmetric gradient coils in MRI. Concept Magn Reson B 2007;31B:218–236.
9. Jackson JM, Forbes LK, While PT, Brideson MA. Could image processing enable reduced acoustic noise during MRI scans. Concept Magn Reson B 2011;39B(4):191–205.
10. Hedeen RA, Edelstein WA. Characterization and prediction of gradient acoustic noise in MR imagers. Magn Reson Med 1997;37: 7–10.
11. Hennel F, Girard F, Loenneker T. "Silent" MRI with soft gradient pulses. Magn Reson Med. 1999;42:6–10.
12. Wu Y, Chronik BA, Bowen C, Mechefske CK, Rutt BK. Gradient-induced acoustic and magnetic field fluctuations in a 4T whole-body MR imager. Magn Reson Med 2000;44:532–536.
13. J. Smink, G-J Plattel, PR Harvey, P Limpens. General methods for acoustic noise reduction by avoiding resonance peaks. In Proceedings of the 16th Annual Meeting of ISMRM, Berlin, Germany, 2007, p. 1088.
14. Schmitter S, Bock M. Acoustic noise-optimized VERSE pulses. Magn Reson Med 2010;64:1446–1452.
15. Li W, Mechefske CK, Gazdzinski C, Rutt BK. Acoustic noise analysis and prediction in a 4-T MRI scanner. Concept Magn Reson B 2004;21B:19–25.
16. More SR, Lim TC, Li M, Holland CK, Boyce SE, Lee J-H. Acoustic noise characteristics of a 4 Telsa MRI scanner. J Magn Reson Imag 2006;23:388–397.
17. Sierra CVR, Versluis MJ, Hoogduin JM, Duifhuis H. Acoustic fMRI noise: linear time-invariant system model. IEEE Bio-Med Eng 2008;55:2115–2123.
18. Segbers M, Rizzo Sierra CV, Duifhuis H, Hoogduin JM. Shaping and timing gradient pulses to reduce MRI acoustic noise. Magn Reson Med 2010;64:546–553.
19. Itakura F, Saito S, An analysis-synthesis telephony based on maximum likelihood method. In Proceedings of 6th International of Congress on Acoustics, Tokyo, 1968, pp. c17–c20.